Self-Assembly of Gold Nanoparticles With Oppositely Charged, Long, Linear Chains of Periodic Copolymers

Nathalie Bridonneau, Vincent Noel, Samia Zrig, and Florent Carn

Self-Assembly of Gold Nanoparticles With Oppositely Charged, Long, Linear Chains of Periodic Copolymers

N. Bridonneau,[1,2] V. Noël,[2] S. Zrig[2*] and F. Carn[1*]

[1] Université de Paris, Laboratoire Matière et Systèmes Complexes, CNRS, UMR 7057, Paris, France.
[2] Université de Paris, ITODYS, CNRS, UMR 7086, 15 rue J-A de Baïf, F-75013 Paris, France

[*] E-mail : florent.carn@univ-paris-diderot.fr, samia.zrig@univ-paris-diderot.fr

Abstract

We studied the assembly of nanoparticles with oppositely charged linear and periodic copolymers (CPs), alternating ionic and polar sequences, in the dilute range of polymer concentration. For the first time, we considered CPs displaying a contour length much higher than the AuNP perimeter. We assumed that such CPs will enable to collect a finite number of NPs into linear nanostructures with a gain of colloidal stability and a better structural control compared to electrostatic complexes obtained with homo polyelectrolytes. As a case study, we synthesized anionic gold nanoparticles (AuNPs) and CPs consisting of alternated cationic poly-L-lysine (PLL) blocks and polar sequences of poly(ethyleneglycol) (PEG). We showed that complexation of AuNPs with CPs is quite similar to that observed with homo PLL. In that respect, finite size nanometric clusters, of less than 30 NPs, outside the electro neutrality domain and a fast phase separation occurs at the electro neutrality. Nevertheless, the presence of PEG blocks allowed us to highlight some specific effects. First, the global charge of the positively charged clusters was found to be always lower for CP based clusters than for homo PLL with a dependence of the charge with the number and the mass of the PEG blocks. Second, in spite of this effect which should have promoted the formation of dense structure, the fractal dimension characterizing the structure of the clusters in bulk was found to be always below 1.8. Finally, we showed that PEG blocks influence the interparticle distance by disfavoring plasmon delocalization when the clusters are dispersed in water and collapse around the nanoparticles when the clusters are deposited on substrate.

1. Introduction

Well-defined clusters of nanoparticles (NPs) mimicking the molecular structure of polymers, so-called colloidal polymers,[1] have drawn attraction in recent years because of the opportunity to access collective properties that are different to those of individual nanoparticles.[2–4] Methodology to self-assemble metal NPs has thus emerged in the last years as a strategy to control the properties of an ensemble of clustered NPs.[1,5–7] In the case of plasmonic NPs the localized surface plasmon resonances of adjacent NPs are coupled when they are in close contact, resulting in the enhancement of the electric field in the gap and the amplification of the optical absorption above 700 nm. Such assemblies are mainly exploited for light to heat conversion,[3,4] the amplification of optical signals (i.e. fluorescence, Raman)[8] and as plasmonic waveguides[9,10]. As pointed by recent simulations[3,11] and experiments[12] on nanoparticles deposited on planar substrate, linear "colloidal oligomers" containing less than 20 gold NPs or opened structures including linear chain fragments could enable to maximize the normalized light absorption efficiency per nanoparticle at $\lambda > 700$ nm compared to dense 3D or 2D clusters. This is relevant for a range of biomedical applications (photo-thermal therapy, bio-imaging, bio-sensing, gene or drug delivery, nano-surgery)[3,4,11] which must deal with toxicity and economical cost by achieving adequate amplification of optical absorption per NPs at a given wavelength and laser power.

In contrast with 3D and also 2D colloidal assembly,[13] it remains a challenge to assemble in bulk a limited number of isotropic nanoparticles (NPs) into 1D structures, similar to linear "colloidal oligomers", using a scalable method based on biocompatible components in water without external forces due to the lack of directional interactions between isotropic NPs. The assembly of charged NPs along oppositely charged biopolymers displaying contour length (L_c) much higher than NP perimeter could be a credible alternative to methods usually reported in the context of colloidal polymers synthesis.[1] Indeed, it has been shown that the electrostatic complexation of cationic gold NPs (AuNPs) with DNA enables to assemble a finite number of NPs in stable linear nanostructures in water by simple mixing.[14] Similar results were then reported with silica NPs[15] and other polyelectrolytes such as chitosan,[16,17] hyaluronic acid,[18,19] polystyrene sulfonate[20] and polylysine.[18] However, as shown theoretically[21] and experimentally[18], the interparticle distance within these assemblies is governed by the electrostatic interactions. Control of the plasmon coupling between adjacent NPs is then made difficult at fixed conditions of electrostatic screening as encountered in biological applications.

Moreover, it was also shown that the structure,[18] aggregation number[22] and stability[21,22] of such assemblies are also influenced by the screening conditions.

To reduce the influence of the ionic strength on the stability and the structure of the clusters, we propose here to assemble anionic AuNPs with long, linear, and periodic copolymers alternating cationic and polar sequences. Although, electrostatic complexation between charged NPs and short copolymers, like diblocks and triblocks, has been extensively studied, the potential of long copolymer chains with contour length much higher than NP perimeter has never been studied so far.[23] We anticipated that, at low concentration, such long copolymers would behave as an homo-polyelectrolyte according to what has been predicted for comb-like polymers at low grafting rate and with small grafts compared to the backbone contour length.[24] As shown in the scheme 1, the flexible ionic segments are expected to wrap around oppositely charged nanoparticles[25] leading to a high cohesion energy per segment/nanoparticle complex while the polar sequences are expected to set the interparticle spacing and to improve the stability of the whole cluster. Previous studies performed on cells and *in vivo* with individual NPs covered by short PEGylated copolymers revealed that this kind of molecule could also increases the colloidal stability in biofluids.[26–28]

As a case study, we considered a linear periodic copolymer (noted CP) composed of PolyEthylene Glycol and Poly-L-Lysine blocks (Scheme 1). This biocompatible polymer was used to assemble in a controlled manner anionic gold nanoparticle (AuNPs) through electrostatic interactions. The potential of this copolymer to assemble AuNPs in "colloidal oligomers" has been studied as a function of the block mass and the number of blocks (n) by combining electrophoretic mobility measurements, dynamic light scattering, small angle X-Ray scattering, UV-Vis. spectroscopy and SEM-FEG observations. AuNPs complexation with a linear homo Poly-L-Lysine (noted homo PLL) was considered as a reference. To the best of our knowledge, this is the first time that the potential of linear periodic copolymers, with contour length higher than the perimeter of the nanoparticle, to collect several nanoparticles per chains is investigated.
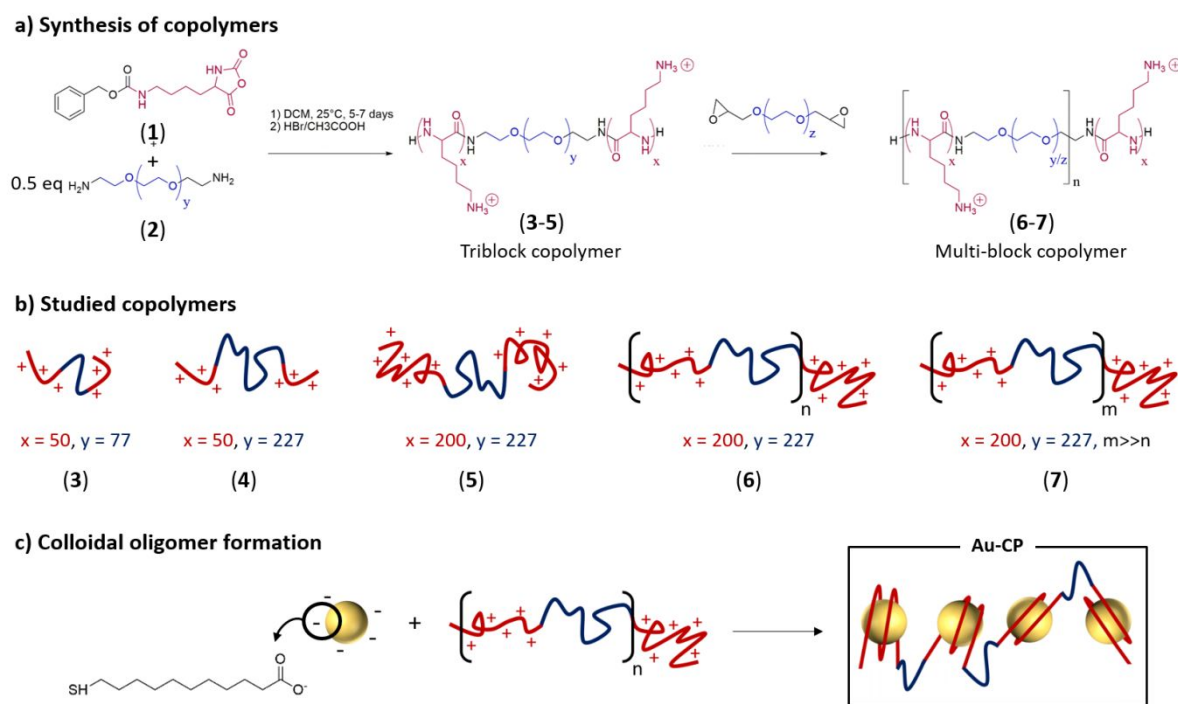
Scheme 1. (a) General synthesis route for the polylysine-poly(ethyleneglycol) copolymers **3-7** (b) Schematic representation of the synthesized polymers. (c) Schematic representation of the colloidal oligomer formation by electrostatic complexation between copolymer and gold nanoparticles functionalized with a self-assembled monolayer of mercaptoundecanoic acid.

2. Experimental Section

Materials. Gold (III) chloride trihydrate (HAuCl$_4$.3H$_2$O, > 99.99 %), trisodium citrate dihydrate (Na$_3$C$_6$H$_5$O$_7$·2H$_2$O, ≥ 99 %) and Ludox® AM colloidal silica (noted Si **1** in the following), were purchased from Sigma-Aldrich and used as received without further purification. Silica nanoparticles Snowtex® ST-O (noted Si **2** in the following) and Snowtex® ST-ZL(noted Si **3** in the following) were a gift from Nissan Chemical Industries Ltd., Tokyo, Japan. All the content of a gold salt powder batch was used at the first opening to prepare, using a glass spatula, a mother solution at 10 g/L in milliQ water that was stocked for period not exceeding 3 months in a dark area to minimize photo-induced oxidation. The same batch of trisodium citrate has been used for all syntheses; it has been stored in desiccators after first opening. All glassware and teflon-coated magnetic bars were washed thoroughly with freshly prepared aqua regia and rinsed with milliQ water after each synthesis. All solutions were prepared with milliQ water (R = 18.2 MΩ). Methanesulfonyl chloride, triphosgene, triethylamine, dihydroxy-PEG of various molar mass (PEG-3400 and PEG-10000), Poly-L-lysine (M$_w$ 150-300

4

kg/mole) and polyethyleneglycol diglycidyl ether (M_n 500) were purchased from Sigma-Aldrich and used as received. CBz-lysine was obtained from Acros Organics.

Nanoparticles synthesis. Citrate stabilized gold nanoparticles were first synthesized by seeded growth protocol.[29,30] Briefly, 97 mg of trisodium citrate (0.33 mmol) were put in 150 mL of water (2.2 mM solution) and refluxed for 15 min, before adding 1 mL of a 10 g/L solution of $HAuCl_4 \cdot 3H_2O$. The solution was kept on reflux for 10 min, then the heating was stopped and the solution was slowly cooled down to 90°C, leaving the reaction mixture in the oil bath. The seeds had their size increased by repeating several growing cycles as followed: 55 mL of the solution were withdrawn, followed by the addition of 53 mL of water and 1 mL of a 60 mM trisodium citrate solution. As soon as the temperature reached 90 °C again, 1 mL of $HAuCl_4 \cdot 3H_2O$ (10 g/L) were added and the solution was stirred for 30 min. Then, another portion of 1mL of $HAuCl_4 \cdot 3H_2O$ were added and the solution was stirred again for 30 min. These growing cycles were repeated up to the desired size of AuNPs. Typically, 4 cycles were required to obtain the desired particles diameter. The replacement of citrate ligand by 11-mercaptoundecanoic acid (MUA) was achieved in two steps by adapting a protocol from literature.[31] Typically, 15 mL of AuNP(citrates) were put in a vial and 0.15 mL of a 0.5 M KOH solution were added. Then, 1.5 mL of α-lipoic acid (10 mM solution) were added and the reaction was stirred overnight. The mixture was centrifuged (15000 rpm, 30 min) and the supernatant discarded. The gold nanoparticles were resuspended in milliQ water and 0.15 mL of 0.5 M KOH were added, followed by 1.5 mL of 11-mercaptoundecanoic acid. The solution was kept stirring overnight before being centrifuged again. The supernatant was discarded and the AuNP(MUA) were kept in solution at the desired concentration. The UV-vis spectrum shows a slight widening of the SPR band upon ligand exchange (see SI). The nanoparticles were concentrated by ultracentrifugation up to a final concentration of 9.6×10^{12} NPs.mL^{-1} (1.6×10^{-8} mol.L^{-1}). For simplicity, the obtained AuNP(MUA) are named AuNPs thereafter.

Polymer syntheses. The polymer syntheses were adapted from literature.[32,33] Details of the synthesis can be found in the supporting information.

Methods.

^{1}H NMR spectra were recorded on a Bruker Advance III spectrometer operating at 400 MHz.

Dynamic light scattering (DLS) experiments were carried out with a NanoZS apparatus (Malvern Instrument) operating at $\lambda = 632.8$ nm and $P \leq 4$ mW. The scattered was measured at

173 °. Data analysis was carried out by converting the measured intensity autocorrelation function into the scattered electric field autocorrelation function using the Siegert relation. The electric field autocorrelation functions were further analyzed by regularized inverse Laplace transformation using the program CONTIN by S. Provencher to yield the distribution of relaxation times (τ).

Laser Doppler velocimetry. Electrophoretic mobility (μ) was measured with a NanoZS apparatus (Malvern Instrument). This set-up operates with an electrical field of 25 V.cm^{-1} oscillating successively at 20 Hz and 0.7 Hz to reduce the electroosmosis effect due to the surface charge of the capillary cell. The particle' velocity was measured by LASER Doppler velocimetry.

Ultraviolet visible spectroscopy (UV-vis) was performed on Cary 50 Scan UV-Visible spectrophotometer (Varian). The diluted AuNPs were filled in the 5 mm thickness Hellma cell (quartz). The absorbance values were recorded after baseline correction.

Small angle X-ray scattering (SAXS) experiments were performed on SWING beamline (SOLEIL synchrotron, Saint-Aubin, France). The configuration was: sample-to-detector distances, D = 6.52 m, beam energy of 12 keV. The samples were contained in cylindrical glass capillaries of calibrated diameter. The scattered signal was recorded by an Eiger 4 M detector (DectrisLtd, Switzerland) with pixel size 75 μm. Preliminary data treatment (angular averaging and normalization) was done using the software Foxtrot developed at the beamline. Subsequent data modelling was done in using SAS View 4.1.2 software.

Scanning electronic microscopy with a field emission gun (SEM-FEG) images of the deposited nanoparticles were obtained using a SEM-FEG Zeiss Merlin Compact with a resolution of 1-2 nm at 10 kV. All images are displayed without any post processing.

3. Results and discussion

3.1 Synthesis of individual partners.

Citrate-stabilized gold nanoparticles were first synthesized in aqueous medium by seeded growth process. Citrate were then replaced by a 11-mercaptoundecanoic acid (MUA) self-assembled monolayer in a two-step process as described by S.Y Lin *et al.*,[31] using α-lipoïc acid as an intermediate ligand. As obtained nanoparticles, noted AuNP(MUA), were finally concentrated by centrifugation up to a final concentration of 9.62×10^{12} NPs.mL^{-1}. After dispersion in MilliQ water at 9.62×10^{11} NP.mL^{-1}, DLS measurements revealed a single population of NPs with $R_H = 28.0 \pm 7.8$ nm (Figure S1a). As expected, such AuNP(MUA) dispersed at pH = 6.5 were negatively charged with an averaged electrophoretic

6

mobility, $\mu = -2.78 \times 10^{-8}$ m^{2}V^{-1}s^{-1} (Figure S1b), that can be related to a ζ -potential of -39 $\pm$ 4 mV according to the Debye−Hückel model. The as-obtained red dispersion displays a surface plasmon resonance (SPR) absorption band at 527 nm (Figure S1c). A more accurate determination of the size distribution was obtained by SEM-FEG and small angle X-Ray scattering (SAXS). The SAXS pattern obtained for a dilute dispersion of AuMUA (Figure S1d) was well fitted by the form factor P(q) of spheres with R = 12.6 $\pm$ 1.9 nm. The slight intensity upturn observed at low q indicates the presence of small NP clusters. One can estimate an average aggregation number of two NPs/clusters by dividing the total scattered intensity by the form factor of individual NPs. Accordingly, SEM-FEG observations (Figures S1e and S1f) revealed isotropic nanoparticles with R = 12.7 $\pm$ 0.1 nm.

In this work, an ensemble of 5 copolymers, numbered from **3** to **7**, was synthesized for the complexation with gold nanoparticles (Scheme 1 and Table 1). The same synthetic strategy was used for the design of the triblock copolymers (polylysine-poly(ethyleneglycol)-polylysine, abbreviated PLL-PEG-PLL) **3**, **4** and **5** which differ by the mass of the different blocks. The synthesis consists in reacting a protected-lysine-N-carboxyanhydride (lysine-NCA) with an amino- functionalized poly(ethyleneglycol) NH$_2$-PEG-NH$_2$ polymer, as depicted on Scheme 1 and ESI. The reaction follows a ring-opening polymerization of the protected aminoacid-NCA, which is a commonly employed method that affords a synthesis of polyamino acids with controllable degrees of polymerization and polydispersity indices.[34] After completion of the reaction the polymer was deprotected by acidic treatment, then purified by dialysis methods. Varying the length of the initial PEG chain (Mw = 3400 and 10000 g/mol) and the lysine-NCA / PEG ratio (100/1 or 400/1) enabled to get several polymers of different molecular weight as summarized in Table 1. Multi block copolymers **6** and **7** were prepared by treating above mentioned triblock copolymers with 0.5 equivalent of polyethyleneglycol diglycidyl ether (Mw = 500 g/mol) at two different concentrations. All polymers were dialyzed in water (MWCO: 1kDa) and obtained as fluffy white powders upon lyophilization. Details of the synthesis can be found in the supporting information.

Polymer	x	y	n	R_H (nm)	ζ (mV)
PLL	1560	0	0		
CP 3	50	77	1	79	17.9
CP 4	50	227	1	97	25.5
CP 5	200	227	1	166	29.2
CP 6	200	227	10	279	48.3
CP 7	200	227	20	400	53.3

7

Table 1. Molecular characteristics of the copolymers (CPs) synthesized in this work and of the commercial poly-L-Lysine (PLL).

3.2 Complexation between AuNP(MUA) and polymers.

The dispersions of Au-CPs and Au-PLL, obtained by simple equivolumic mixing, were first studied for $[AuNPs] = 2.04 \times 10^{-9}$ mol/L by electrophoretic mobility measurements (Figure 1a) and DLS (Figure 1b) on several decades of relative molar ratio χ, with $\chi = \dfrac{n_{AuNPs}/n_{CPs}}{\left(n_{AuNPs}/n_{CPs}\right)_{\mu\,=\,0\,m^2V^{-1}s^{-1}}}$. We observed that finite size nanometric complexes (Figure 1b) with negative or positive global charge (Figure 1a) were already formed 2 min after mixing at low and high molar ratio whatever the nature of the polymers. The main impact of the polymer nature has been observed for $\chi \leq 0.5$ where the Au-CPs complexes present an averaged ζ potential increasing from + 13 to + 31 mV with the degree of polymerization of the CPs while the hydrodynamic size remain almost constant. By comparison the ζ potential of Au-PLL complexes is around + 40 mV. This result may be understood by considering the picture of complexes with pearl necklace structure where one pearl is composed of PLL wrapped around one AuNP. This kind of structure was reported experimentally and theoretically for electrostatic complexes of nanoparticles and polymers.[14,15,21,25] In this view, electrophoretic mobility measurements are sensitive to the total charge of the pearl necklace which is the sum of the pearls charge and the charge of the polymer segments separating the pearls. The difference between the complexes obtained with CPs and with pure PLL should come from the contribution of the chain segments separating the pearls which are fully charged for Au-PLL and partially charged for Au-CPs due to PEG contribution. In the case of Au-CPs, the effect of the degree of polymerization should be understood by considering that the number of positive charges per chains increases with the degree of polymerization, from polymer **3** to **7**, so that "pearl" overcharging must increases with the degree of polymerization. In any cases, the global charge of the complexes in this domain (i.e. $\chi \leq 0.5$) and the presence of PEG blocks are sufficient to enable their stabilization in aqueous media beyond a few days.

Moreover, all the samples (i.e. Au-CPs and Au-PLL dispersions) were destabilized with the formation of micrometric clusters that sediment beyond few hours at the charge stoichiometry ($\chi = 1$).

These results show that, contrary to our initial expectation, the presence of PEG segments with mass comprised between 3400 and 10 000 g/mole does not enable to improve the stability of the neutral complexes. For $\chi \geq 3$, the complexes prepared with a same batch of

AuNPs present almost the same size and zeta potential up to $\chi = 100$: $\langle \zeta \rangle = -39 \pm 4$ mV and $\langle R_H \rangle = 57 \pm 10$ nm whatever the nature of the CPs. The complexes prepared by combining CP **4** with another batch of AuNPs (Figure S2) present different characteristics from previous complexes with $\langle \zeta \rangle = -36 \pm 4$ mV and $\langle R_H \rangle = 40 \pm 10$ nm. This shows that the characteristics of the complexes are governed by the nanoparticles and hardly affected by the nature of the complexing agent in this domain where negative charges are in excess.
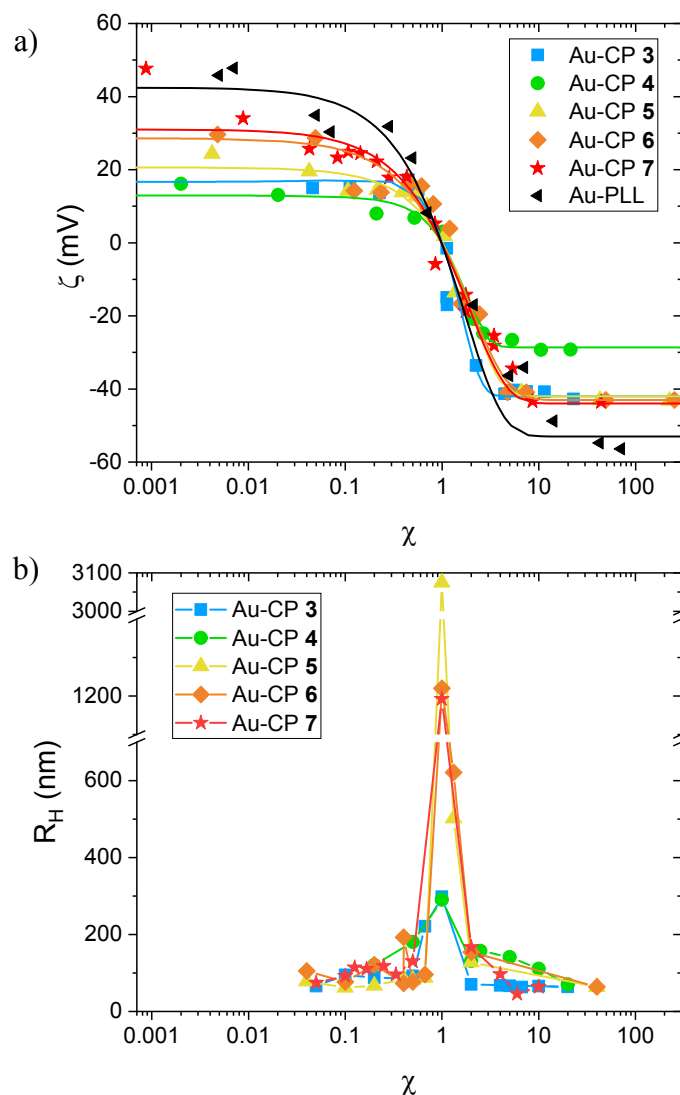

Figure 1. (a) Evolution of the zeta potentials (ζ) and (b) hydrodynamic radii (R_H) upon colloidal oligomer formation using the five synthesized PEG-PLL copolymers **3** (blue square), **4** (green disk), **5** (yellow triangle), **6** (orange diamond), **7** (red star) and the commercial PLL homopolymer (black triangle). All the experiments were done with the same batch of nanoparticles described in Figure S1 except for PEG-PLL copolymers **4** (Figure S2).

In a second step we tried to see to what extent the evolution of the electrophoretic mobility with the partner ratio, $\mu(\chi)$, was dependent on the characteristics of the nanoparticles. In this issue, we considered commercial silica nanoparticles (SiNPs) with different sizes: Si **1**

9

(R_H = 8 nm, figure 2a), b) Si **2** (R_H = 14 nm, figure 2b) and c) Si **3** (R_H = 65 nm, figure 2c) as shown in figure S4. We underline that the structural surface charge density (σ) of these particles is much lower than the one of AuMUA with $\sigma_{SiNP} \approx 0.4$ e/nm² and $\sigma_{AuMUA} \approx 4$ e/nm².
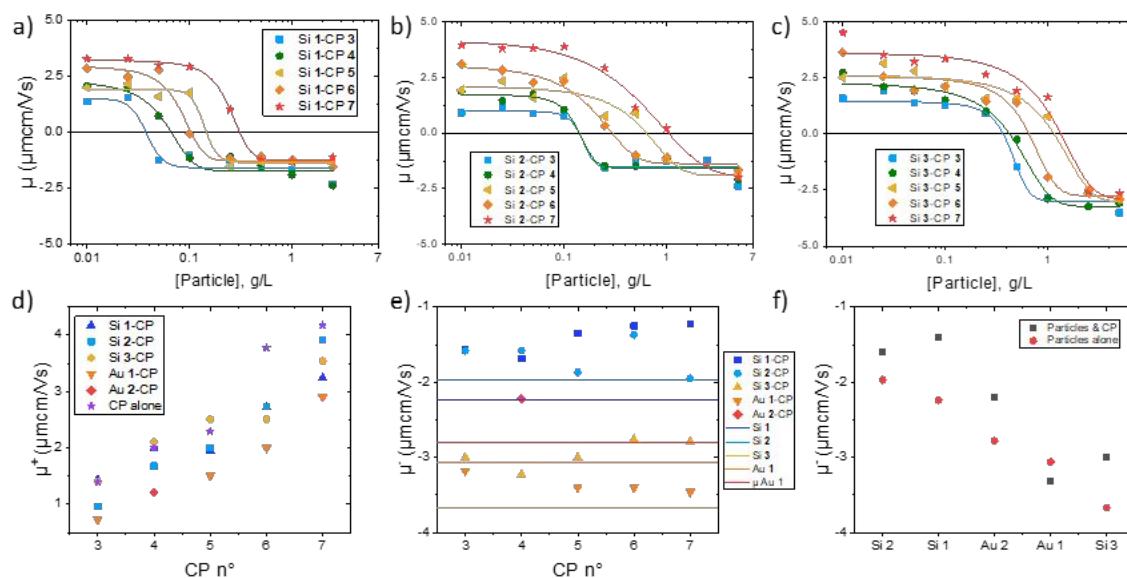

Figure 2. Evolution of the electrophoretic mobility (μ) upon colloidal oligomer formation using the five synthesized PEG-PLL copolymers at fixed concentration (c = 0.025 g/L) and three kinds of silica nanoparticles: a) Si **1** (R_H = 8 nm), b) Si **2** (R_H = 14 nm) and c) Si **3** (R_H = 65 nm). Evolution of the averaged electrophoretic mobility of cationic (d) and anionic (e) complexes as a function of the nature of the copolymer. (f) Evolution of the averaged electrophoretic mobility of anionic complexes as a function of the nature of the nanoparticles.

These measurements confirm that the charge of cationic complexes is driven by the nature of the CPs and increases as the mass and overall charge of CPs increases. The surface charge density of the particles also seems to have an effect on the overall charge of complexes in this domain since the charges obtained with gold particles are always lower than those obtained with silica particles as shown in figure 2d. In contrast, our measurements do not reveal a significant role of particle size in the probed size range (i.e. 8 < R (nm) < 65). Conversely, the charge of the anionic complexes is almost independent of CP' nature (figure 2e) and highly dependent of the particle' nature (figure 2f).

In addition, we tried to see if the measured charge stoichiometries for these different pairs of particles and CPs (Figure 3) corresponded to our expectations on the basis of the supposed structural charges of the two partners. It turned out that the measured charge stoichiometries are obtained for charge ratios [+] / [-] higher or lower by a factor ~ 7 than those expected from our calculations. This shift is significant but not aberrant in view of the uncertainty on the structural charge of the particles and has already been observed for systems involving homo

10

polyelectrolytes of high mass and/or high charge density (i.e. subject to Manning condensation like poly-L-lysine).[20]
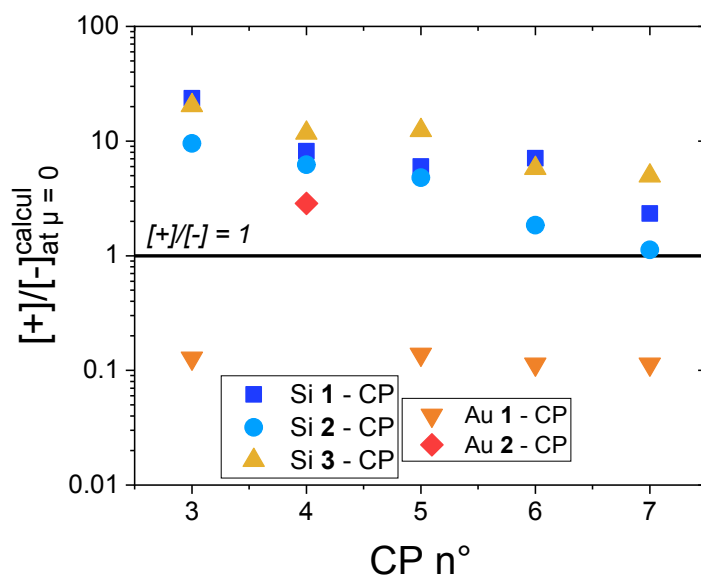

Figure 3. Evolution of the structural charge ratios [+] / [-] calculated at the measured charge stoechiometries for the different couples of CPs and particles. We considered $\sigma_{AuMUA} \approx 4$ e/nm², $\sigma_{AuMUA} \approx 0.4$ e/nm² and 1 e/lysine for the calculations.

The structure of the Au-CPs and Au-PLL complexes was investigated by small-angle X-ray scattering (SAXS). Figure 4 shows typical scattering curves from complexes obtained for $\chi < 0.3$ (Figure 4a) and for $\chi > 3$ (Figure 4b). Overall, the scattering curves appeared similar for the different Au-CPs and for the Au-PEL self-assemblies whatever the χ value. One detects the form factor of individual nanoparticles at high q followed at low q (i.e. $q < 0.002$ Å^{-1}) by a power law variation of the scattered intensity on at least one decade with an exponent (i.e. mass fractal dimension, D_f) comprised between 1.2 and 1.8 corresponding to somehow elongated and branched clusters. Going into more details, some specific features appear. For $\chi > 3$ (Figure 4b), the structure of the complexes (i.e. Au-CPs and Au-PLL) is somehow independent of the nature of the polymer with $D_f \approx 1.4$. When χ is decreased below 0.3, the fractal dimension of Au-PLL decreases while the opposite effect is observed for all Au-CPs. Hence, Au-CPs complexes are denser, with $1.6 \leq D_f \leq 1.8$, than Au-PLL complexes with $D_f \approx 1.2$. Moreover, D_f increases from 1.6 to 1.8 when the CP' degree of polymerization increases as shown in the inset of figure 4a. This effect is slight, but has been observed for the three ratios studied below 0.3. We underline that the fractal dimension obtained with Au-PLL agrees with previous experimental[18] and numerical[35] studies dedicated to the structural evolution of nanoparticle/homo-polyelectrolyte complexes as a function of the ratio between the polyelectrolyte total persistence

length (L_T) and the radius of the nanoparticles. Indeed, such studies predicted a transition toward linear structures when $L_T/R > 1$ as observed here with:

$$\frac{L_T}{R} = \frac{L_0 + L_e}{R} = \frac{L_0 + {}^1\!/_{4\kappa^2 l_B}}{R} \approx \frac{1 + {}^1\!/_{(4 \times 0.1^2 \times 0.7)}}{12.6} \approx 3$$

where $L_0 \approx 1$ nm is the intrinsic persistence length of PLL and L_e is the electrostatic persistence length, which depends on the inverse Debye screening length (κ) , and the Bjerrum length (l_B) as proposed by Odijk[36] and Skolnick and Fixman[37] in the case where Manning's counterion condensation occurs. Interestingly, the presence of non-ionic PEG blocks affects the transition toward straight 1D structures (i.e. $D_f = 1$). This could be understood by considering that the electrostatic repulsion between segments of the same charge, at the basis of L_e, within complexes is an important ingredient of this transition.
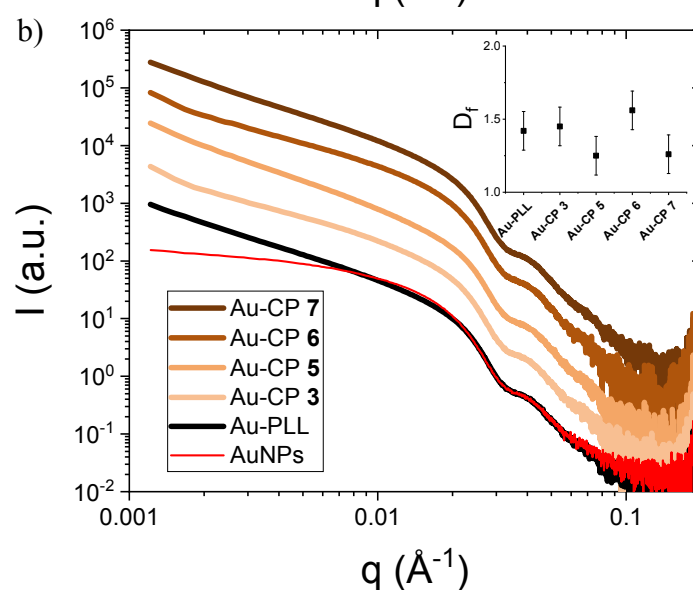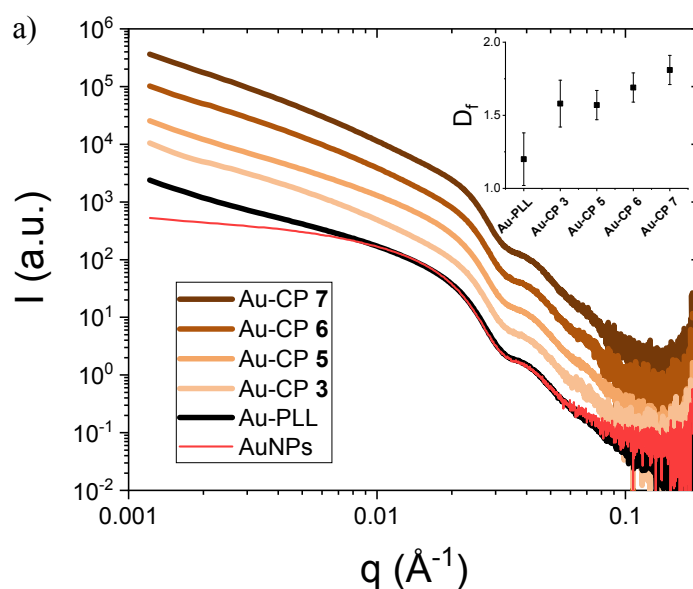
Figure 4. Typical SAXS curves obtained for dilute dispersions of Au-CPs and Au-PLL prepared 2 min before the measurements at (a) $\chi < 0.3$ and (b) $\chi > 3$. The inset represents the evolution of the mass fractal dimensions determined at $q < 0.02$ Å^{-1}.

The interparticle distance within clusters is not accessible on the SAXS curves due to a probable structural polydispersity. We performed simple UV-Vis. spectroscopy (Figure 5) to shed light on this parameter through the detection of a collective absorption band arising from plasmonic coupling at short interparticle distance. Overall, the complexation with CPs leads to a widening of the localized surface plasmon resonance (LSPR) band of individual AuNPs around 525 nm when χ goes towards 1 while remaining outside the electro neutrality domain. In the neutrality domain (i.e. $\chi \approx 1$), a second SPR band grows around 600 nm and evolves concomitantly with the primary LSPR band. In contrast, for Au-PLLs, a distinct secondary SPR band could be detected above 600 nm on the whole χ range. We analyze these results by considering that the presence of a secondary SPR band with a maximum at $\lambda \geq 600$ nm results from plasmon delocalization on the different particles of a given complex. Considering that the complexes have almost the same structure whatever the nature of the polymer (Figure 6), we believe that plasmon coupling is less good for Au-CPs than for Au-PLL due to a greater interparticle distance. Indeed, the PEG blocks should contribute to the particle separation in addition to the electrostatic repulsion. The widening of the LSPR band and the eventual emergence of a second SPR band when χ goes towards 1 should reflect the reduction of the electrostatic contribution to the interparticle distance.
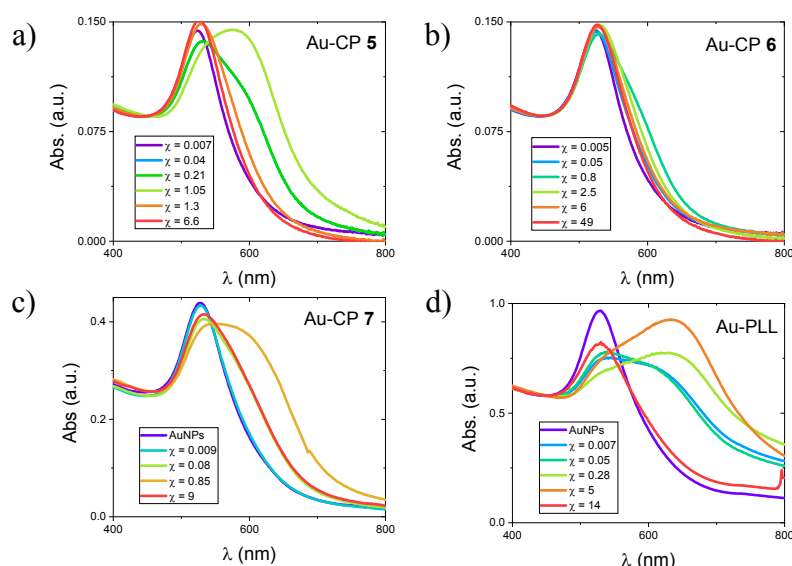

Figure 5. Absorbance spectra of (a) Au-CP **5**, (b) Au-CP **6**, (c) Au-CP **7** and (d) Au-PLL. The samples were prepared at different χ and studied 2 min after mixing. Spectra were normalized at 450 nm to facilitate comparison.

Finally, the structure of Au-CPs has been observed with SEM-FEG after deposition and drying on planar substrates (Figure 4). We underline that this technique can hardly account for the structure of the complexes in solution, as described by SAXS, but it seemed interesting to us to characterize the objects in this way, given the potential applications of nanoparticles deposited on model surfaces. As a reminder, in absence of polymer, at the concentration of ~ 10^{12} NPs/mL, the particles are mainly individual with some dimers and trimers where particles are in close contact. In presence of CPs, the particles are aggregated in small clusters with an aggregation number always below ~ 30 NPs. The structure of these clusters after surface deposition and drying is opened. Apart from their sizes, these clusters differ from those detected in absence of polymers by the presence of a visible polymeric shell which was never detected so far in the case of complexes involving homo polyelectrolytes.[16,17] Interestingly, the interparticle distance is small compared to the particle size despite this polymeric shell that should result from the collapse of PEG blocks upon drying. Additional images of the Au-CPs are displayed in the supporting information (Figure S3).
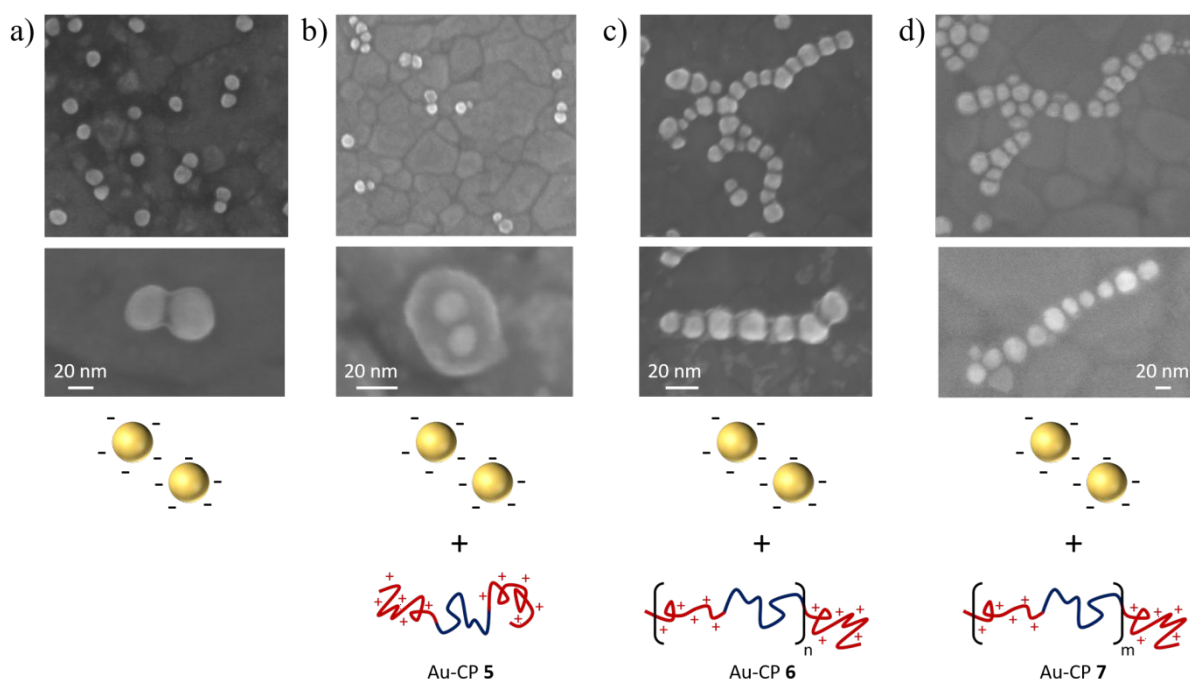

Figure 6. Typical SEM-FEG images of dried patterns obtained after deposition and drying of (a) AuMUA, (b) Au-CP **5**, (c) Au-CP **6** and (d) Au-CP **7** dispersions. The colloidal oligomers were prepared at $0.2 < \chi < 0.6$, 2 min before deposition.

4. Conclusion

In summary, periodic copolymers (CPs) composed of PolyEthylene Glycol / Poly-L-Lysine blocks were synthesized and used to assemble gold nanoparticle (AuNPs) through

electrostatic interactions between Poly-L-Lysine (PLL) and the anionic coating of the AuNPs. We considered a linear homo PLL as reference and 5 CPs with blocks of different masses and number of blocks. This family of polymers allowed us, for the first time, to study the capacity of periodic copolymers, with contour length higher than the perimeter of the nanoparticle, to collect several NPs per chains and thus to form colloidal oligomers. From a general point of view, we showed that complexation of AuNPs with CPs is similar to that observed with homo PLL. In that respect, finite size nanometric clusters of NPs were always formed outside the electro neutrality domain and a fast phase separation occured at the electro neutrality. Indirectly, this shows that these copolymers, whose conformation in water has never been studied, have probably a similar behavior to that of homo polyelectrolytes. Nevertheless, the presence of the PEG blocks allowed us to highlight some specific effects. First, the global charge of the positively charged clusters was found to be always lower for CP based clusters than for homo PLL based clusters with a dependence of the charge with the number and the mass of the PEG blocks. Second, in spite of this effect, which should have promoted the formation of dense structure, the fractal dimension characterizing the structure of the clusters is always below 1.8 whatever the polymer nature. Moreover, in contrast with our initial expectation, we did not detect any stabilizing effect of PEG blocks notably at the electro neutrality. Finally, we showed that PEG blocks influence the interparticle distance by disfavoring plasmon delocalization when the clusters are dispersed in water and collapse around the nanoparticles when the clusters are deposited on substrate.

We hope that this first physical insight concerning the electrostatic complexation of NPs with long chains of periodic copolymers prone to form colloidal oligomers with better control than with homo polyelectrolytes will encourage the development of this type of assembly which could be of general interest given its simplicity and biocompatibility.

5. Supporting Information. Characterizations of the nanoparticles and polymers by dynamic light scattering, scanning electronic microscopy, ^{1}H NMR and laser Doppler electrophoresis. Additional elements concerning the synthesis protocol of the different polylysine-poly(ethyleneglycol) copolymers. Additional SEM-FEG images of colloidal oligomer obtained at χ<1 using AuMUA and copolymer **5**, **6** and **7.**

7. References

(1) Hill, L. J.; Pinna, N.; Char, K.; Pyun, J. Colloidal Polymers from Inorganic Nanoparticle Monomers. *Prog. Polym. Sci.* **2015**, *40*, 85–120.

(2) Halas, N. J.; Lal, S.; Chang, W.-S.; Link, S.; Nordlander, P. Plasmons in Strongly Coupled Metallic Nanostructures. *Chem. Rev.* **2011**, *111*, 3913–3961.

(3) Khlebtsov, B.; Zharov, V.; Melnikov, A.; Tuchin, V.; Khlebtsov, N. Optical Amplification of Photothermal Therapy with Gold Nanoparticles and Nanoclusters. *Nanotechnology* **2006**, *17*, 5167–5179.

(4) Baffou, G.; Quidant, R. Thermo-Plasmonics: Using Metallic Nanostructures as Nano-Sources of Heat: Thermoplasmonics. *Laser & Photon. Rev.* **2013**, *7*, 171–187.

(5) Slaughter, L. S.; Willingham, B. A.; Chang, W.-S.; Chester, M. H.; Ogden, N.; Link, S. Toward Plasmonic Polymers. *Nano Lett.* **2012**, *12*, 3967–3972.

(6) Klinkova, A.; Choueiri, R. M.; Kumacheva, E. Self-Assembled Plasmonic Nanostructures. *Chem. Soc. Rev.* **2014**, *43*, 3976.

(7) Bouju, X.; Duguet, É.; Gauffre, F.; Henry, C. R.; Kahn, M. L.; Mélinon, P.; Ravaine, S. Nonisotropic Self-Assembly of Nanoparticles: From Compact Packing to Functional Aggregates. *Adv. Mater.* **2018**, *30*, 1706558.

(8) Freeman, R. G.; Grabar, K. C.; Allison, K. J.; Bright, R. M.; Davis, J. A.; Guthrie, A. P.; Hommer, M. B.; Jackson, M. A.; Smith, P. C.; Walter, D. G.; et al. Self-Assembled Metal Colloid Monolayers: An Approach to SERS Substrates. *Science* **1995**, *267*, 1629–1632.

(9) Ebbesen, T. W.; Genet, C.; Bozhevolnyi, S. I. Surface-Plasmon Circuitry. *Phys. Today* **2008**, *61*, 44–50.

(10) Lin, S.; Li, M.; Dujardin, E.; Girard, C.; Mann, S. One-Dimensional Plasmon Coupling by Facile Self-Assembly of Gold Nanoparticles into Branched Chain Networks. *Adv. Mater.* **2005**, *17*, 2553–2559.

(11) Onal, E. D.; Guven, K. Plasmonic Photothermal Therapy in Third and Fourth Biological Windows. *J. Phys. Chem. B* **2017**, *121*, 684–690.

(12) Barrow, S. J.; Funston, A. M.; Gómez, D. E.; Davis, T. J.; Mulvaney, P. Surface Plasmon Resonances in Strongly Coupled Gold Nanosphere Chains from Monomer to Hexamer. *Nano Lett.* **2011**, *11*, 4180–4187.

(13) Boles, M. A.; Engel, M.; Talapin, D. V. Self-Assembly of Colloidal Nanocrystals: From Intricate Structures to Functional Materials. *Chem. Rev.* **2016**, *116*, 11220–11289.

(14) Keren, K.; Soen, Y.; Yoseph, G. B.; Gilad, R.; Braun, E.; Sivan, U.; Talmon, Y. Microscopics of Complexation Between Long DNA Molecules and Positively Charged Colloids. *Phys. Rev. Lett.* **2002**, *89* 088103.

(15) Zinchenko, A. A.; Yoshikawa, K.; Baigl, D. Compaction of Single-Chain DNA by Histone-Inspired Nanoparticles. *Phys. Rev. Lett.* **2005**, *95*, 228101.

(16) Shi, L.; Carn, F.; Boué, F.; Mosser, G.; Buhler, E. Nanorods of Well-Defined Length and Monodisperse Cross-Section Obtained from Electrostatic Complexation of Nanoparticles with a Semiflexible Biopolymer. *ACS Macro Lett.* **2012**, *1*, 857–861.

(17) Shi, L.; Carn, F.; Boue, F.; Mosser, G.; Buhler, E. Control over the Electrostatic Self-Assembly of Nanoparticle Semiflexible Biopolyelectrolyte Complexes. *Soft Matter* **2013**, *9*, 5004–5015.

(18) Shi, L.; Carn, F.; Boue, F.; Buhler, E. Role of the Ratio of Biopolyelectrolyte Persistence Length to Nanoparticle Size in the Structural Tuning of Electrostatic Complexes. *Phys. Rev. E* **2016**, *94*, 032504.

(19) Carn, F.; Guyot, S.; Baron, A.; Perez, J.; Buhler, E.; Zanchi, D. Structural Properties of Colloidal Complexes Between Condensed Tannins and Polysaccharide Hyaluronan. *Biomacromolecules* **2012**, *13*, 751–759.

(20) Shi, L.; Buhler, E.; Boue, F.; Carn, F. Shape-Tailored Colloidal Molecules Obtained by Self-Assembly of Model Gold Nanoparticles with Flexible Polyelectrolyte. *Langmuir* **2015**, *31*, 5731–5737.

(21) Nguyen, T. T.; Shklovskii, B. I. Complexation of a Polyelectrolyte with Oppositely Charged Spherical Macroions: Giant Inversion of Charge. *J. Chem. Phys.* **2001**, *114*, 5905–5916.

(22) Sennato, S.; Truzzolillo, D.; Bordi, F. Aggregation and Stability of Polyelectrolyte-Decorated Liposome Complexes in Water–Salt Media. *Soft Matter* **2012**, *8*, 9384.

(23) Chapel, J.-P.; Berret, J.-F. Versatile Electrostatic Assembly of Nanoparticles and Polyelectrolytes: Coating, Clustering and Layer-by-Layer Processes. *Curr. Opin. Colloid Interface Sci.* **2012**, *17*, 97–105.

(24) Gay, C.; Raphaël, E. Comb-like Polymers inside Nanoscale Pores. *Adv. Colloid Interface Sci.* **2001**, *94*, 229–236.

(25) Netz, R.; Joanny, J.-F. Complexation Between a Semiflexible Polyelectrolyte and an Oppositely Charged Sphere. *Macromolecules* **1999**, *32*, 9013-9025.

(26) Torrisi, V.; Graillot, A.; Vitorazi, L.; Crouzet, Q.; Marletta, G.; Loubat, C.; Berret, J.-F. Preventing Corona Effects: Multiphosphonic Acid Poly(Ethylene Glycol) Copolymers for Stable Stealth Iron Oxide Nanoparticles. *Biomacromolecules* **2014**, *15*, 3171–3179.

(27) Ramniceanu, G.; Doan, B.-T.; Vezignol, C.; Graillot, A.; Loubat, C.; Mignet, N.; Berret, J.-F. Delayed Hepatic Uptake of Multi-Phosphonic Acid Poly(Ethylene Glycol) Coated Iron Oxide Measured by Real-Time Magnetic Resonance Imaging. *RSC Adv.* **2016**, *6*, 63788–63800.

(28) Giamblanco, N.; Marletta, G.; Graillot, A.; Bia, N.; Loubat, C.; Berret, J.-F. Serum Protein-Resistant Behavior of Multisite-Bound Poly(Ethylene Glycol) Chains on Iron Oxide Surfaces. *ACS Omega* **2017**, *2*, 1309–1320.

(29) Bastús, N. G.; Comenge, J.; Puntes, V. Kinetically Controlled Seeded Growth Synthesis of Citrate-Stabilized Gold Nanoparticles of up to 200 Nm: Size Focusing versus Ostwald Ripening. *Langmuir* **2011**, *27*, 11098–11105.

(30) Shi, L.; Buhler, E.; Boue, F.; Carn, F. How Does the Size of Gold Nanoparticles Depend on Citrate to Gold Ratio in Turkevich Synthesis? Final Answer to a Debated Question. *J. Colloid Interface Sci.* **2017**, *492*, 191–198.

(31) Lin, S.-Y.; Tsai, Y.-T.; Chen, C.-C.; Lin, C.-M.; Chen, C. Two-Step Functionalization of Neutral and Positively Charged Thiols Onto Citrate-Stabilized Au Nanoparticles. *J. Phys. Chem. B* **2004**, *108*, 2134–2139.

(32) Gu, P. F.; Xu, H; Sui, B. W.; Gou, J. X.; Meng, L. K.; Sun, F.; Wang, X. J.; Qi, N.; Zhang, Y.; He, H. B; et al.Polymeric Micelles Based on Poly(Ethylene Glycol) Block Poly(Racemic Amino Acids) Hybrid Polypeptides: Conformation-Facilitated Drug-Loading Behavior and Potential Application as Effective Anticancer Drug Carriers. *Int. J. Nanomed.* **2012**, *7*, 109-122.

(33) Sui, B.; Xu, H.; Jin, J.; Gou, J.; Liu, J.; Tang, X.; Zhang, Y.; Xu, J.; Zhang, H.; Jin, X. Self-Assembled Micelles Composed of Doxorubicin Conjugated Y-Shaped PEG-Poly(Glutamic Acid)2 Copolymers via Hydrazone Linkers. *Molecules* **2014**, *19*, 11915–11932.

(34) Skepö, M.; Linse, P. Complexation, Phase Separation, and Redissolution in Polyelectrolyte−Macroion Solutions. *Macromolecules* **2003**, *36*, 508–519.

(35) Odijk, T. Polyelectrolytes near the Rod Limit. *J. Polym. Sci. Pol. Phys.* **1977**, *15*, 477–483.

(36) Skolnick, J.; Fixman, M. Electrostatic Persistence Length of a Wormlike Polyelectrolyte. *Macromolecules* **1977**, *10*, 944–948.

17

1
2
3
4
5
6
7
8
9
10
11
12
13
14
15
16
17
18
19
20
21
22
23
24
25
26
27
28
29
30
31
32
33
34
35
36
37
38
39
40
41
42
43
44
45
46
47
48
49
50
51
52
53
54
55
56
57
58
59
60

TOC Graphic